Optimization-based Planning and Control of Quadrupedal Robot Walking on Dynamic Rigid Surfaces ⋆

Amir Iqbal * and **Yan Gu** *

* *University of Massachusetts Lowell, Lowell, MA 01854, USA (e-mail: amir_iqbal@student.uml.edu and yan_gu@uml.edu).*

Abstract: Stabilizing legged robot locomotion on a dynamic rigid surface (DRS) (i.e., rigid surface that moves in the inertial frame) is a complex planning and control problem. The complexity arises due to the hybrid nonlinear walking dynamics subject to explicitly time-varying holonomic constraints caused by the surface movement. The first main contribution of this study is the extension of the capture point from walking on a static surface to locomotion on a DRS as well as the use of the resulting capture point for online motion planning. The second main contribution is a quadratic-programming (QP) based feedback controller design that explicitly considers the DRS movement. The stability and robustness of the proposed planning and control method are validated through simulations of a quadrupedal robot walking on a DRS with a rocking motion. The simulation results also demonstrate the improved walking performance compared with our previous approach based on offline planning and input-output linearizing control that does not explicitly guarantee the feasibility of ground contact constraints.

Keywords: Motion Control Systems, Legged Locomotion, Motion Planning, Dynamic Modeling, Quadratic Programming

1. INTRODUCTION

Legged robots, mimicking nature's design of terrestrial animals, have many potential advantages compared to wheeled or tracked robots in traversing unstructured terrains. Various planning and control methods have been created and successfully implemented to enable stable and robust locomotion on stationary surfaces (Kuindersma et al., 2016; Hutter et al., 2016; Bledt et al., 2018). Yet, sustaining legged locomotion on a non-stationary surface has not been fully addressed. The objective of this study is to derive a planning and control approach that stabilizes locomotion on a dynamic rigid surface (DRS) by explicitly addressing the time-varying surface movement and the feasibility of ground contact forces. A key element of the proposed approach is an online footstep planner that considers the surface motion through the extension of the concept of capture point (Pratt et al., 2006; Koolen et al., 2012) from stationary to dynamic surfaces. Another key element is a quadratic programming (QP) based control method that incorporates the surface motion in its constraints. Related work is reviewed next.

1.1 Related work on Planning and Control of Legged Locomotion on Rigid Stationary and Deformable Surfaces

Previous planner and controller designs for legged robot locomotion mainly focus on static (flat or uneven) platforms (e.g., pavement, stairs, and gravels) (Kajita et al., 2003; Chevallereau et al., 2009; Gu et al., 2018; Gao and Gu, 2019; Barasuol et al., 2013; Hutter et al., 2016; Gao and Gu, 2019). For example, robust quadrupedal locomotion on stationary surfaces has been experimentally demonstrated on various physical robots (Hutter et al., 2016; Bledt et al., 2018; Lee et al., 2020). Yet, these controllers may not work well for locomotion on a deformable surface or a DRS because they do not explicitly account for perturbations to the robot motion caused by the surface deformation or movement.

One of the pioneering efforts in addressing locomotion on deformable surfaces (e.g., sand and snow) is the modeling of the dynamic interaction between the robot's legs and granular terrains (e.g., sands) (Li et al., 2013). Based on this model, Xiong et al. (Xiong et al., 2017) have developed a stability region criterion for granular terrain walking to guide controller design. Recently, a learning-based controller has been derived and experimentally demonstrated to realize robust locomotion on highly unstructured, deformable terrains (Lee et al., 2020). However, it is unclear how effective these methods would be for sustaining locomotion on a DRS.

1.2 Related Work on Planning and Control of Legged Locomotion on a DRS

Stabilizing legged locomotion on a DRS is fundamentally challenging due to the high complexity of the associated robot dynamics. First, the robot dynamics are inherently hybrid involving state-triggered discrete behaviors (e.g., foot touchdowns) (Galeani et al., 2011). Second, without properly addressed, the time-varying perturbation at a foot-surface contact point caused by the surface motion can destabilize the robot.

Recently, planning and control of DRS locomotion have been drawing an increasing attention. For surfaces with a motion affected by the locomotor (e.g., passive surfaces with relatively small inertia), a reduced-order model based planning and control method for bipedal walking on different-sized balls has been studied (Zheng and Yamane, 2011). A model predictive

⋆ Research by A. Iqbal and Y. Gu was supported in part by NSF under Grant no. CMMI-1934280. Corresponding author: Y. Gu.

control (MPC) method based on full-order dynamic modeling has been introduced to stabilize locomotion on a moving ball and to manipulate the ball over the ground (Yang et al., 2020). Also, modeling and control of legged locomotion on a floating island have been proposed based on an eight-legged rimless wheel robot model (Asano, 2021). However, these methods cannot be directly used to handle locomotion on a DRS whose motion is not affected by the robot due to the differences in the associated robot dynamics.

To address locomotion on a DRS whose motion is not affected by the robot (e.g., vessels and aircraft), our previous work has analyzed the effects of surface movement on a robot's locomotion stability based on the reduced-order spring-loaded inverted pendulum (SLIP) robot model (Iqbal et al., 2021). Furthermore, we have recently created and experimentally evaluated a provably stabilizing controller for enabling quadrupedal locomotion on such a DRS (Iqbal et al., 2020). Yet, this controller has two major limitations towards effective implementation in a real-world scenario. First, the planning algorithm is offline and cannot be used for online motion generation due to the heavy computational load caused by its underlying full-order model. Second, the control does not explicitly account for the feasibility of ground-contact constraints during the actual walking process.

1.3 Related Work on Capture Point

A capture point is defined as the point that an inverted pendulum model needs to instantaneously extend its leg in order to come to a complete stop within the new step (Pratt et al., 2006). Based on the capture point, Capturability has been introduced to describe a robot's ability to come to a complete stop given its current state and has been widely used as a measure of locomotion stability (i.e., the ability not to fall over) (Koolen et al., 2012). Due to its computational efficiency, the concept of capture point has been used to plan footsteps for legged locomotion on static surfaces (Englsberger et al., 2011; Pratt et al., 2012). It has also been proven effective in planning and control of legged locomotion on uneven terrains (Morisawa et al., 2012; Caron et al., 2019) as well as disturbance rejection (Pratt et al., 2012; Joe and Oh, 2018). However, to the best of our knowledge, the capture point has not been extended to solve the footstep planning problem of a robot walking on a DRS.

1.4 Related Work on QP-based Locomotion Planning and Control

Due to its capability of incorporating feasibility constraints and its low computational load suitable for real-time implementation, QP-based motion planning and control design have been extensively studied for legged locomotion (Focchi et al., 2017; Carpentier et al., 2017; Bledt et al., 2018). Hardware experiments under QP-based controllers that utilize reduced-order robot model have shown robust performance in moving over high-slope terrains (Focchi et al., 2017) and unstructured terrains (Bledt et al., 2018). Recently, a QP-based controller utilizing a full-order robot model has shown effectiveness in robustly tracking desired trajectories (Hamed et al., 2020). Still, these controllers do not explicitly consider the time-varying surface motion during DRS locomotion, which may deteriorate locomotion performance and even cause instability.

1.5 Contributions

This paper aims to derive a planning and control approach that enables stable and robust quadrupedal walking on a DRS by extending our previous work (Iqbal et al., 2020) and solving its two major limitations, which are: a) lack of feasibility guarantees in the controller design and b) the heavy computational load of motion planning that prevents real-time planning.

The main contributions of this paper include:

a) Extending the concept of capture point to DRS locomotion by explicitly considering the surface movement, and designing a real-time footstep planner based on the extended capture point.
b) Formulating a QP-based controller that ensures the feasibility of ground contact forces and explicitly incorporates the surface motion in a time-varying holonomic constraint.
c) Validating the stability and robustness of the proposed approach through simulations of quadrupedal robot walking on a DRS with a periodic, rocking motion.
d) Providing comparative simulation results to demonstrate the improved robustness of the proposed method over our previous work.

2. HYBRID FULL-ORDER ROBOT MODEL

This section presents the full-order model of a quadrupedal robot that walks on a DRS, which captures the complete dynamic behaviors of all degrees of freedom (DOFs) of the robot. The model is used as a basis for the proposed QP-based controller design.

A walking robot's dynamics are hybrid because walking naturally involves continuous-time motion (e.g., foot swinging) and discrete events (e.g., foot touchdowns). A complete cycle of quadrupedal walking is illustrated in Fig. 1, which consists of four continuous phases connected by four instantaneous foot touchdown events. During locomotion on a DRS, the robot's dynamics are also affected the time-varying movement of the surface, which is modeled as a time-varying holonomic constraint in this study. The hybrid, time-varying robot dynamics are explained next.

2.1 Continuous-Phase Dynamics

Let $\mathbf{q}$ be the generalized coordinates of a robot, which consists of the robot's base pose (i.e., position and orientation) and joint angles and is defined as:

$$\mathbf{q} := \left[\mathbf{p}_b^T,\ \boldsymbol{\gamma}_b^T,\ q_1,\ q_2,\ ...,\ q_n\right]^T, \tag{1}$$

where the vectors $\mathbf{p}_b$ and $\boldsymbol{\gamma}_b$ are the base position and orientation in the world frame, respectively, the vector $[q_1\ q_2\ ...\ q_n]^T$ is the joint angles, and $\mathcal{Q} \subset \mathbb{R}^{n+6}$ is the robot's configuration space. Let $\mathbf{u} \in U \subset \mathbb{R}^m$ be the robot's joint torques with U the admissible set of joint torques.

Using Lagrange's method, continuous-phase robot dynamics can be obtained as:

$$\mathbf{M}(\mathbf{q})\ddot{\mathbf{q}} + \mathbf{C}(\mathbf{q},\dot{\mathbf{q}}) := \mathbf{B}\mathbf{u} + \mathbf{J}_f^T(\mathbf{q})\mathbf{F}_f, \tag{2}$$

where $\mathbf{M}(\mathbf{q}) : \mathcal{Q} \to \mathbb{R}^{(n+6)\times(n+6)}$ is the inertia matrix, $\mathbf{C}(\mathbf{q},\dot{\mathbf{q}}) : \mathcal{TQ} \to \mathbb{R}^{(n+6)}$ represents the sum of centrifugal, Coriolis, and gravitational terms with $\mathcal{TQ}$ the tangent space of $\mathcal{Q}$, and $\mathbf{B} \in$

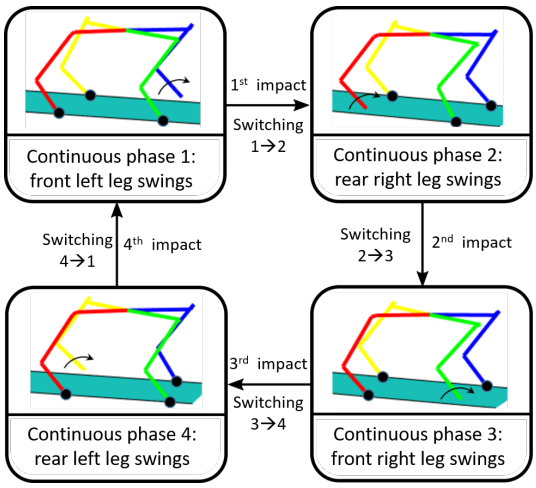

Fig. 1. A complete cycle of quadrupedal walking (Iqbal et al., 2020).

$\mathbb{R}^{(n+6)\times m}$ is the actuator selection matrix. The matrix $\mathbf{J}_f(\mathbf{q})$ is the contact Jacobian whose expression varies during different phases because of different feet in support (see Fig. 1). The vector $\mathbf{F}_f(\mathbf{q}) \in \mathbb{R}^{n_{ct}}$ represents the external force acting at the support feet. During three-dimensional (3-D) quadrupedal walking without slip, three of the four legs are in secured contact with the surface, and therefore $n_{ct} = 9$.

During robot walking on a DRS whose motion is not affected by the robot, the effects of the surface motion on the robot dynamics can be modeled as a time-varying holonomic constraint.

Let $\mathbf{r}_p(t) \in \mathbb{R}^{n_{ct}}$ be the positions of the surface at the support-foot locations. Note that for a DRS, the surface positions and motions at the foot-contact points (i.e., $\mathbf{r}_p(t)$ and its derivatives) are explicitly time-varying. Let $\mathbf{r}_f(\mathbf{q}) \in \mathbb{R}^{n_{ct}}$ be the positions of the support feet. Then, the contact Jacobian matrix, by definition, is expressed as $\mathbf{J}_f(\mathbf{q}) := \frac{\partial \mathbf{r}_f}{\partial \mathbf{q}}(\mathbf{q})$.

When there is no relative motion between support feet and the surface, the time-varying holonomic constraint is given by:

$$\mathbf{J}_f(\mathbf{q})\ddot{\mathbf{q}} + \dot{\mathbf{J}}_f((\mathbf{q}),\dot{\mathbf{q}})\dot{\mathbf{q}} = \ddot{\mathbf{r}}_p(t). \tag{3}$$

2.2 Switching Surface

When a swing foot strikes the walking surface, it becomes a new stance foot while another foot begins to swing in the air and acts as the new swing foot. $S := \{(\mathbf{q},\dot{\mathbf{q}},\mathbf{r}_f,\dot{\mathbf{r}}_f) \in \mathcal{TQ} \times \mathbb{R}^{n_{ct}} \times \mathbb{R}^{n_{ct}} : \phi(\mathbf{q},\mathbf{r}_f) = 0,\ \dot{\phi}(\mathbf{q},\dot{\mathbf{q}},\mathbf{r}_f,\dot{\mathbf{r}}_f) < 0\}$, where the scalar function ϕ is the distance between the swing foot and the surface.

3. CAPTURE-POINT BASED ONLINE MOTION PLANNING

This section introduces the extension of the capture point from stationary to DRS walking, as well as the proposed online planning method based on the extended capture point. The desired trajectories produced by the planner will be tracked by the proposed QP-based control as introduced in Sec. 4.

3.1 Capture Point on a DRS

The concept of capture point for a static surface has been extensively studied (Pratt et al., 2006; Koolen et al., 2012). In this work, we extend the capture point to a DRS based on a reduced-order locomotor model, that is, a 2-D linear inverted pendulum model (LIPM) with a point mass atop a massless leg (see Fig. 2). The position of the point mass coincides with its center of mass (CoM).

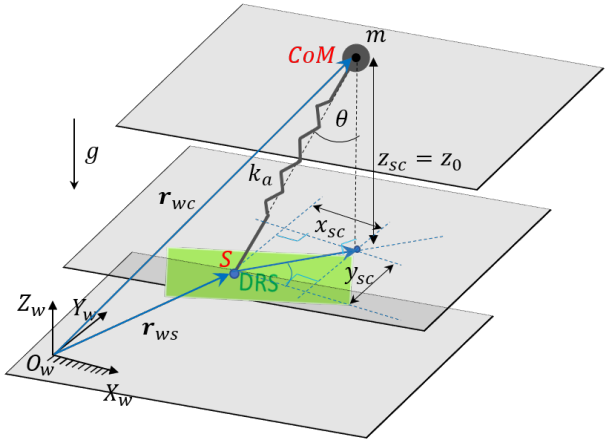

Fig. 2. Illustration of the 3-D LIPM model on a DRS. The model is constrained to maintain constant height z_0 between the CoM and the point S on the DRS.

Let $\mathbf{r}_{wc} = (x_{wc},\ x_{wc},\ z_{wc})$ and $\mathbf{r}_{ws} = (x_{ws},\ x_{ws},\ z_{ws})$ be the absolute positions of the CoM and the leg's far end (i.e., point S) in the world frame, respectively.

$$\mathbf{r}_{sc} = (x_{sc},\ x_{sc},\ z_{sc}) = \mathbf{r}_{wc} - \mathbf{r}_{ws}. \tag{4}$$

The equation of motion of the LIPM is expressed as:

$$\ddot{x}_{wc} = \frac{f_a}{m}\sin\theta\frac{x_{sc}}{r},\ \ddot{y}_{wc} = \frac{f_a}{m}\sin\theta\frac{y_{sc}}{r} \text{ and} \tag{5}$$

$$\ddot{z}_{wc} = \frac{f_a}{m}\cos\theta - g, \tag{6}$$

where m is the mass of the LIPM, θ is the angle of the leg relative to the vertical axis, g is the magnitude of the gravitational acceleration, and r is the projected length of $\mathbf{r}_{sc}$ on the X_wY_w-plane. The scalar variable f_a is the norm of the axial force applied on the point mass by the massless rod.

It is assumed in this study that the vertical distance z_{sc} between the CoM and point S is constant during walking (see Fig. 2); that is, $z_{sc} = z_0$ with z_0 a positive number. This assumption is analogous to the simplifying assumption of the LIPM model on a stationary surface that the point-mass height over the surface is constant (Pratt et al., 2006).

Under the assumption that z_{sc} is constant, $\dot{z}_{wc} = \dot{z}_{ws}$ and $\ddot{z}_{wc} = \ddot{z}_{ws}$. Then, from (6), the expression of f_a in (3.1) becomes $f_a = m\frac{(\ddot{z}_{ws}+g)}{\cos\theta}$. Accordingly, the equation of motion of the LIPM on the horizontal plane is now given by:

$$\ddot{x}_{wc} = (\ddot{z}_{ws}+g)\frac{x_{sc}}{z_0} \text{ and } \ddot{y}_{wc} = (\ddot{z}_{ws}+g)\frac{y_{sc}}{z_0}, \tag{7}$$

From (4), we obtain $\ddot{x}_{wc} = \ddot{x}_{ws} + \ddot{x}_{sc}$ and $\ddot{y}_{wc} = \ddot{y}_{ws} + \ddot{y}_{sc}$. Then, using these relations in (7) yields:

$$\ddot{x}_{sc} - \frac{(\ddot{z}_{ws}+g)}{z_0}x_{sc} = \ddot{x}_{ws},\ \text{and}\ \ddot{y}_{sc} - \frac{(\ddot{z}_{ws}+g)}{z_0}y_{sc} = \ddot{y}_{ws}, \tag{8}$$

Equation (8) is a linear, non-homogeneous 2^{nd}-order ordinary differential equation in x_{sc} and y_{sc}, respectively.

For the case where the acceleration of point S along the X_w and Y_w-directions is sufficiently small (i.e., $\ddot{x}_{ws}$ and $\ddot{y}_{ws}$ are negligible), then the forcing terms $\ddot{x}_{ws}$ and $\ddot{y}_{ws}$ in (8) can be approximated as zero. Then, the ODE becomes homogeneous:

$$\ddot{x}_{sc} - \frac{(\ddot{z}_{ws}+g)}{z_0}x_{sc} = 0 \text{ and } \ddot{y}_{sc} - \frac{(\ddot{z}_{ws}+g)}{z_0}y_{sc} = 0. \quad (9)$$

Analogous to the derivation of the capture point on a stationary surface (Pratt et al., 2006), define the apparent stiffness of the LIPM as $k_a := -\frac{(\ddot{z}_{ws}+g)}{z_0}$. Then, we reduce the LIPM's equation to a spring-mass system with unit mass; that is, $\ddot{x}_{sc}+k_a x_{sc} = 0$ and $\ddot{y}_{sc}+k_a y_{sc} = 0$. The orbital energy of this system associated with x and y-components of motion are given as:

$$E_x = \frac{1}{2}(\dot{x}_{sc}^2 + k_a x_{sc}^2) \text{ and } E_y = \frac{1}{2}(\dot{y}_{sc}^2 + k_a y_{sc}^2), \quad (10)$$

These energy terms predict whether the point mass will move over the support point S (i.e., $E_x + E_y > 0$), stop at S (i.e., $E_x + E_y = 0$), or reverse the direction of motion before reaching S (i.e., $E_x + E_y < 0$).

At the equilibrium (i.e., $E_x = 0$ and $E_y = 0$) of the system in (9), the two eigenvectors are:

$$\dot{x}_{sc} = \pm\sqrt{\frac{(\ddot{z}_{ws}+g)}{z_0}}x_{sc} \text{ and } \dot{y}_{sc} = \pm\sqrt{\frac{(\ddot{z}_{ws}+g)}{z_0}}y_{sc}. \quad (11)$$

The stable eigenvector corresponds to the case when x_{sc} and $\dot{x}_{sc}$ (and y_{sc} and $\dot{y}_{sc}$) have opposite signs, which lead to the following X_w- and Y_w-coordinates of the instantaneous capture point of the 3-D LIPM on a DRS:

$$x_{cap} := \sqrt{\frac{z_0}{(\ddot{z}_{ws}+g)}}\dot{x}_{sc} \text{ and } y_{cap} := \sqrt{\frac{z_0}{(\ddot{z}_{ws}+g)}}\dot{y}_{sc}. \quad (12)$$

The Z_w-coordinate of the instantaneous capture point lies on the DRS. For a horizontal, flat DRS with a constant horizontal velocity but a varying vertical velocity (e.g., elevators), the z-coordinate of the capture point will be zero, i.e., $z_{cap} = 0$.

The capture point $(x_{cap}, y_{cap}, z_{cap})$ is the position of the CoM with respect to a new support point S. Note that this equation will no longer be valid when the term $(\ddot{z}_{wp}+g)$ is negative (i.e., the robot loses contact with the DRS).

Analogous to the capture point on a stationary surface, if the LIPM instantaneously places the far end of its leg (point S) at $(x_{cap}, y_{cap}, z_{cap})$, it will come to a complete stop *relative to the new support point* within the immediate successive step.

The expression of the horizontal coordinates of the capture point in (12) explicitly considers the surface motion that was not incorporated in the previous derivations of the capture point on a stationary surface (Pratt et al., 2006; Caron et al., 2019). Note that when $\ddot{z}_{ws} = 0$, i.e., the surface is stationary or moving with a constant speed in both the horizontal and vertical directions, the proposed capture point on a DRS in (12) reduces exactly to the capture point on a stationary surface.

3.2 Capture-Point based Online Foot-Step Planning

The objective of the proposed footstep planner is to generate a robot's desired foot placement for maintaining a certain desired walking motion *instead of* making the robot to stop. To this end, the capture point $(x_{cap}, y_{cap}, z_{cap})$ is further extended to determine the desired footsteps that help sustain the planned robot movement. For simplicity, the desired motion is specified by a constant base velocity $\mathbf{v}_d = (v_{dx}, v_{dy}, 0)$ relative to point S.

We choose to design the desired foot placement $(\tilde{x}_{step}, \tilde{y}_{step}, \tilde{z}_{step})$ as the difference between the capture point associated with the current relative CoM velocity $\dot{\mathbf{r}}_{sc}$ and a fictitious capture point corresponding to the desired velocity $\mathbf{v}_d$ (Bledt et al., 2018) multiplied by a positive gain K_{step}:

$$\begin{aligned} \tilde{x}_{step} &:= K_{step}\sqrt{\frac{z_0}{(\ddot{z}_{ws}+g)}}(\dot{x}_{sc} - v_{dx}), \\ \tilde{y}_{step} &:= K_{step}\sqrt{\frac{z_0}{(\ddot{z}_{ws}+g)}}(\dot{y}_{sc} - v_{dy}), \text{ and } \tilde{z}_{step} := 0. \end{aligned} \quad (13)$$

The gain can be used to tune how much the difference in the current and desired CoM velocities affects the desired footstep location, thus allowing us to consider practical hardware limitations (e.g., finite step duration and limited leg length) in foot placement planning. For the presented results, we choose K_{step} to be 1.

To ensure that the robot moves with v_{dx} in the X_w-direction, Raibert's heuristic $\frac{T}{2}v_d$ (Bledt et al., 2018) is used along with the instantaneous capture point in (13) to plan the X_w-coordinate of the desired foot placement:

$$x_{step} = x_{hip} + \frac{T}{2}v_{dx} + \tilde{x}_{step}, \quad (14)$$

where x_{hip} is the X_w-coordinate of the swing hip joint and T is the desired duration of a complete gait cycle.

Similarly, the y-coordinate of the desired foot placement in the world frame is given as:

$$y_{step} = y_{hip} + \frac{T}{2}v_{dy} + \tilde{y}_{step}, \quad (15)$$

The z-coordinate of the desired foot placement on a horizontal flat DRS is $z_{step} = \tilde{z}_{step} = 0$. Then, the desired footstep location in the world is: $[x_{\text{step}}\ \ y_{\text{step}}\ \ z_{\text{step}}]^T$.

3.3 Whole-Body Trajectory Generation

This subsection explains the method we adopt to generate the whole-body reference position trajectories.

It is assumed in the planner (and controller) designs that the surface pose and motion are accurately estimated and predicted in real-time. This assumption is reasonable because real-world, man-made platforms such as aircraft and ships are typically equipped with motion monitoring systems that estimate the surface's body motion. The design of such a predictor is not the focus of this study.

The number of reference position trajectories to be planned depends on the robot's DOFs. The robot used in the simulation validation is the Laikago quadrupedal robot with twelve revolute joints (i.e., $n = m = 12$) (Unitree, 2019). The robot has nine DOFs during walking (Iqbal et al., 2020) where three legs are in full, static contact with the surface. Thus, nine reference position trajectories will be planned.

We choose the inputs to the proposed reference trajectory generator as: i) the desired gait duration T, ii) maximum swing-foot height, iii) the desired walking speed, and iv) the current and predicted surface pose and motion. The nine desired trajectories $h_d(t)$ produced by the trajectory generator are: i) the robot's base pose trajectories and ii) swing foot position trajectories.

As various existing methods can be used to design the needed whole-body trajectory generator (Pratt et al., 2012; Caron et al., 2019), we will only highlight how the proposed generator respects the surface motion and desired footsteps. To ensure the robot's desired base pose conforms to the DRS movement, the base pose trajectories are planned online based on the desired walking velocity $\mathbf{v}_d$ as well as the surface pose and motion. To guarantee that the desired swing foot trajectories respect the desired foot placement, they are generated through a smooth interpolation from the actual initial location of a footstep to the desired foot placement (Westervelt et al., 2007).

4. INSTANTANEOUS QP-BASED CONTROLLER DESIGN

This section introduces the proposed QP-based controller design that provably tracks the desired walking motions $\mathbf{h}_d(t)$ on a DRS and guarantees the feasibility for ground contact forces. The QP-based controller is synthesized based on full-order dynamics of a quadruped walking on a DRS, and explicitly addresses the surface movement through the formulation of the holonomic and the friction cone constraints.

Both QP and MPC can be used to formulate a controller with feasibility guarantees. We choose to use QP because its computational load is low enough for the typical real-time controller implementation rate (e.g., 500 Hz or higher) even when the QP is formulated based upon a full-order robot model. In contrast, an MPC synthesized based on a full-order model typically computes its output at a much lower rate, e.g., 30Hz.

The key steps to the proposed QP formulation include the selection of optimization variables and the design of the cost function and constraints, which are explained next.

Optimization variables. As the control objective is to achieve reliable trajectory tracking with the ground contact constraints respected, we define the optimization variables $\mathbf{x}$ as the control input $\mathbf{u}$ and ground contact force $\mathbf{F}_f$, i.e., $\mathbf{x} = [\mathbf{u}^T, \mathbf{F}_c^T]^T$.

Cost function. The quadratic cost function to be minimized is set as $\mathbf{x}^T\mathbf{Q}\mathbf{x} + (\tilde{\mathbf{x}} - \mathbf{x})^T\mathbf{W}(\tilde{\mathbf{x}} - \mathbf{x})$ with $\tilde{\mathbf{x}}$ the values of the optimization variables at the previous optimization step. The weighting matrix $\mathbf{Q}$ is a symmetric, positive definite matrix with an appropriate dimension. The minimization of $\mathbf{x}^T\mathbf{Q}\mathbf{x}$ is to minimize the joint torques The other weighting matrix, $\mathbf{W}$, is a symmetric, positive definite matrix that can be used to penalize sharp variations in some of the optimization variables.

Equality time-varying holonomic constraints: To ensure that the support feet do not move relative to the surface, we consider the time-varying holonomic contraint in (3) that explicitly contains the surface movement.

From the continuous-phase dynamics in (2), we have

$$\ddot{\mathbf{q}} := \mathbf{M}^{-1}(\mathbf{B}\mathbf{u} + \mathbf{J}_f^T\mathbf{F}_f - \mathbf{C}). \tag{16}$$

Plugging it in the holonomic constraint in (3) gives: $\mathbf{J}_f\mathbf{M}^{-1}(\mathbf{B}\mathbf{u} + \mathbf{J}_f^T\mathbf{F}_f - \mathbf{C}) + \dot{\mathbf{J}}_f\dot{\mathbf{q}} = \ddot{\mathbf{r}}_p(t)$, which, upon rearrangement, gives:

$$\mathbf{A}_{eq1}\mathbf{x} = \mathbf{b}_{eq1}, \tag{17}$$

where $\mathbf{A}_{eq1} := [\mathbf{J}_f\mathbf{M}^{-1}\mathbf{B},\ \mathbf{J}_f\mathbf{M}^{-1}\mathbf{J}_f^T]$ and $\mathbf{b}_{eq1} := \mathbf{J}_f\mathbf{M}^{-1}\mathbf{C} - \dot{\mathbf{J}}_f\dot{\mathbf{q}} + \ddot{\mathbf{r}}_p(t)$.

Equality constraints based on input-output linearizing control: To realize accurate tracking of the desired base and swing-foot trajectories $\mathbf{h}_d(t)$, the controller takes the form of an input-output (I-O) linearizing control law (Iqbal et al., 2020) with the output function defined as the tracking error. We choose I-O linearization to form the control law because I-O linearization transforms the nonlinear continuous-phase robot dynamics into a linear one, thus simplifying the controller design.

Let $\mathbf{h}$ denote the variables of interest (i.e., base pose and swing foot position). Then, the output function representing the tracking error is given by:

$$\mathbf{y} := \mathbf{h}(\mathbf{q}) - \mathbf{h}_d(t) \tag{18}$$

Then, $\dot{\mathbf{y}} = \frac{\partial \mathbf{h}}{\partial \mathbf{q}}\dot{\mathbf{q}} - \dot{\mathbf{h}}_d$ and $\ddot{\mathbf{y}} = \frac{\partial}{\partial \mathbf{q}}(\frac{\partial \mathbf{h}}{\partial \mathbf{q}}\dot{\mathbf{q}})\dot{\mathbf{q}} + \frac{\partial \mathbf{h}}{\partial \mathbf{q}}\ddot{\mathbf{q}} - \ddot{\mathbf{h}}_d$. Define $\mathbf{J}_h := \frac{\partial \mathbf{h}}{\partial \mathbf{q}}$, and then $\dot{\mathbf{J}}_h = \frac{\partial}{\partial \mathbf{q}}(\frac{\partial \mathbf{h}}{\partial \mathbf{q}}\dot{\mathbf{q}})$. we get the output function dynamics as $\ddot{\mathbf{y}} = \mathbf{J}_h\ddot{\mathbf{q}} + \dot{\mathbf{J}}_h\dot{\mathbf{q}} - \ddot{\mathbf{h}}_d$.

To stabilize the output function dynamics, we utilizes a proportional-derivative (PD) feedback term as:

$$\ddot{\mathbf{y}} = -\mathbf{K}_p\mathbf{y} - \mathbf{K}_d\dot{\mathbf{y}} =: \mathbf{v}, \tag{19}$$

which, combined with the expression of $\ddot{\mathbf{q}}$ in (16), yields:

$$\mathbf{J}_h\mathbf{M}^{-1}(\mathbf{B}\mathbf{u} + \mathbf{J}_c^T\mathbf{F}_c - \mathbf{C}) + \dot{\mathbf{J}}_h\dot{\mathbf{q}} + \ddot{\mathbf{h}}_d(t) = \mathbf{v}, \tag{20}$$

which can be compactly written as:

$$\mathbf{A}_{eq2}\mathbf{x} = \mathbf{b}_{eq2}, \tag{21}$$

where $\mathbf{A}_{eq2} := [\mathbf{J}_{hc}\mathbf{M}^{-1}\mathbf{B},\ \mathbf{J}_h\mathbf{M}^{-1}\mathbf{J}_f^T]$ and $\mathbf{b}_{eq2} := \mathbf{J}_{hc}\mathbf{M}^{-1}\mathbf{C} - \dot{\mathbf{J}}_h\dot{\mathbf{q}} - \ddot{\mathbf{h}}_d(t) + \mathbf{v}$.

Note that (19) and (20) can be easily rearranged into the expression of the input-output linearizing control law $\mathbf{u}$.

Inequality ground-contact constraints and joint torque limits. To secure contacts between the robot's support feet and the surface, the QP incorporates the following friction cone (i.e., no foot slipping) and unilateral (i.e., no feet penetrating the surface) constraints $\mathbf{F}_f \in \mathcal{F}_{gc}$, where $\mathcal{F}_{gc}$ is the set of ground-contact forces satisfying the friction cone and unilateral constraints. Also, the solution to the QP must satisfy the joint torque limits; i.e., the control input $\mathbf{u}$ must be within the admissible torque set, $\mathbf{u} \in U$.

QP-based control law. With the cost function and constraints designed, the proposed QP can be compactly expressed as:

$$\begin{aligned} \min_{\mathbf{x}} \quad & \mathbf{x}^T\mathbf{Q}\mathbf{x} + (\mathbf{x}_p - \mathbf{x})^T\mathbf{W}(\mathbf{x}_p - \mathbf{x}) \\ \text{subject to} \quad & \mathbf{A}_{eq1}\mathbf{x} = \mathbf{b}_{eq1}, \\ & \mathbf{A}_{eq2}\mathbf{x} = \mathbf{b}_{eq2}, \\ & \mathbf{F}_f \in \mathcal{F}_{gc},\ u \in \mathbf{U}. \end{aligned} \tag{22}$$

Stability property. As proven in our previous study (Iqbal et al., 2020), an input-output linearizing controller with form (19) and (20) can guarantee the (local) asymptotic stability of the desired trajectory $\mathbf{h}_d(t)$ for the hybrid, time-varying walking process, if the PD gains are chosen to render a sufficiently fast error convergence rate during continuous phases.

5. SIMULATIONS

This section presents MATLAB simulation results that validate the effectiveness of the proposed planning and control method during unperturbed (Case 1) and perturbed (Case 2) walking.

5.1 Simulation setup

Robot. The robot model used for the simulation validation is a Laikago quadruped developed by Unitree (Unitree, 2019). Its

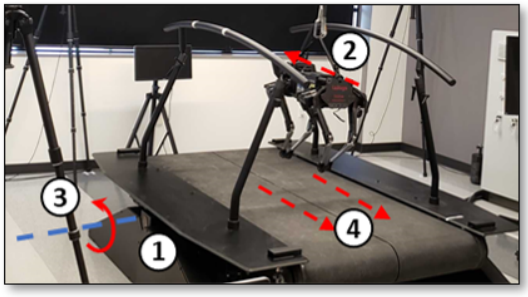

Fig. 3. System setup that the simulator emulates. The treadmill ① has a split belt ④ that moves at a constant speed of 8cm/s while the treadmill undergoes a sinusoidal rocking motion about the horizontal axis ③. The quadruped is a Laikago robot ②.

total mass is 25 kg, and each leg weighs 2.9 kg. Every leg has three independently actuated joints (i.e., hip-roll, hip-pitch, and knee-pitch), with torque limits of 20 Nm, 55 Nm, and 55 Nm, respectively. The overall length, width, and height of the robot are 0.56m, 0.35m, and 0.60m, respectively.

Surface. The simulated DRS is an actuated platform (see Fig. 3) simultaneously experiencing: a) a whole-body sinusoidal pitching motion, with a amplitude of $\pm 5^\circ$ and a pitching frequency of 0.5 Hz, and b) a constant surface translating motion. This DRS reasonably satisfies the assumption underlying the proposed capture point extension, because the horizontal velocity of the surface is approximately constant due to the small pitching amplitude. The surface acceleration in the vertical direction is still relatively significant for the validation of the proposed method.

QP-based controller. The PD gains are $\mathbf{K}_p = 120\mathbf{I}_9$ and $\mathbf{K}_d = 22\mathbf{I}_9$, where $\mathbf{I}_n$ is an $n \times n$ identity matrix. The weighting matrices in the cost function are set as: $\mathbf{Q} = \text{blockdiag}(1000\mathbf{I}_{12},\ \mathbf{I}_9,)$ and $\mathbf{W} = \text{blockdiag}(10^{-1}\mathbf{I}_{12},\ 10^{-4}\mathbf{I}_9,)$. The torque bounds are set based on the robot's hardware limits. In the unilateral constraint, the lower bound of the normal ground reaction force at a support foot is set as 1 N. In the friction cone constraint, the friction coefficient is chosen as 0.5.

Planner. The inputs to the planner are: a) desired gait cycle $T =$ 2s, b) maximum swing foot height 15 cm, c) desired walking speed 8 cm/s, and d) the surface movement as explained earlier.

5.2 Results

Case 1 (unperturbed walking). Figure 4 shows the simulation results of robot walking on the DRS without perturbations under the proposed planning and control method. As shown in Fig. 4 (c), the base height is relatively constant, and the base orientation mildly varies, indicating that the proposed method can sustain stable walking on the DRS in the absence of perturbations. Also, Figs. 4 (a) and (b) show that the joint torques are within the limits and the ground contact constraints are satisfied.

Case 2 (perturbed walking). Figures 5 and 6 display the simulation results of robot walking on the DRS under sinusoidal perturbation forces applied at the center of the robot's base. The magnitude of the external force is:

$$F_p(t) = \begin{cases} 30sin(2\pi t)\ \text{N} & \text{if } 2\text{s} \le t \le 4\text{s} \\ 0\ \text{N} & \text{otherwise} \end{cases} \quad (23)$$

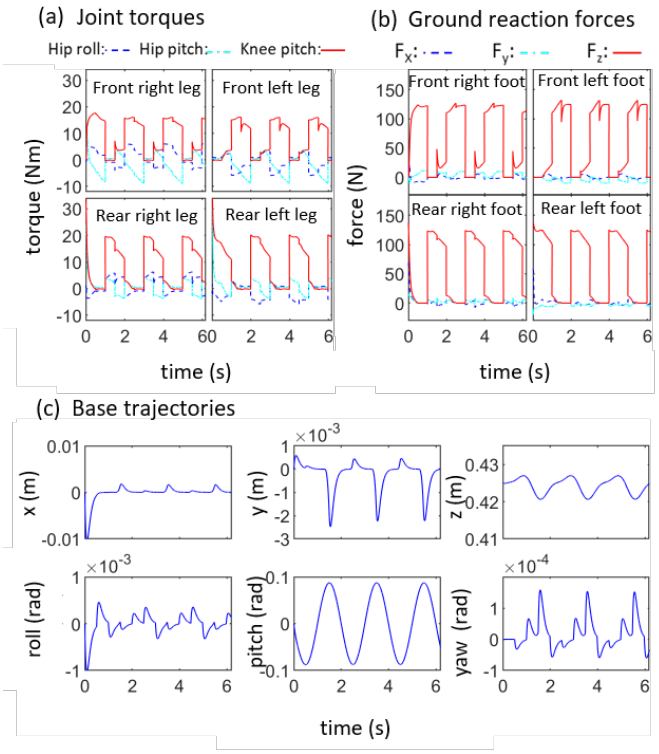

Fig. 4. Simulation results obtained from unperturbed walking (Case 1): (a) joint torques, (b) ground reaction forces, and (c) base trajectories

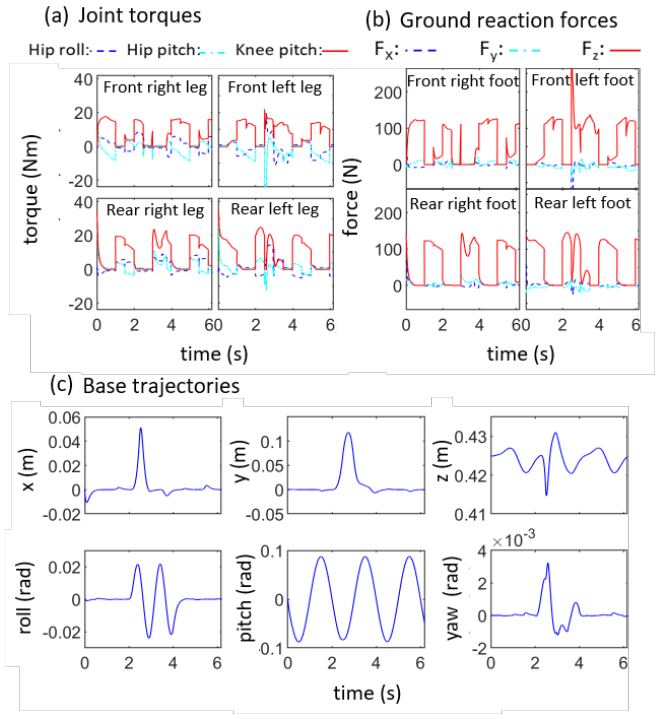

Fig. 5. Simulation results obtained from Case 2 with lateral perturbations: (a) joint torques, (b) ground reaction forces, and (c) base trajectories.

Two types of perturbations are simulated: (1) perturbation applied in the lateral Y_w-direction (Fig. 5) and (2) perturbation applied in the forward walking X_w-direction (Fig. 6).

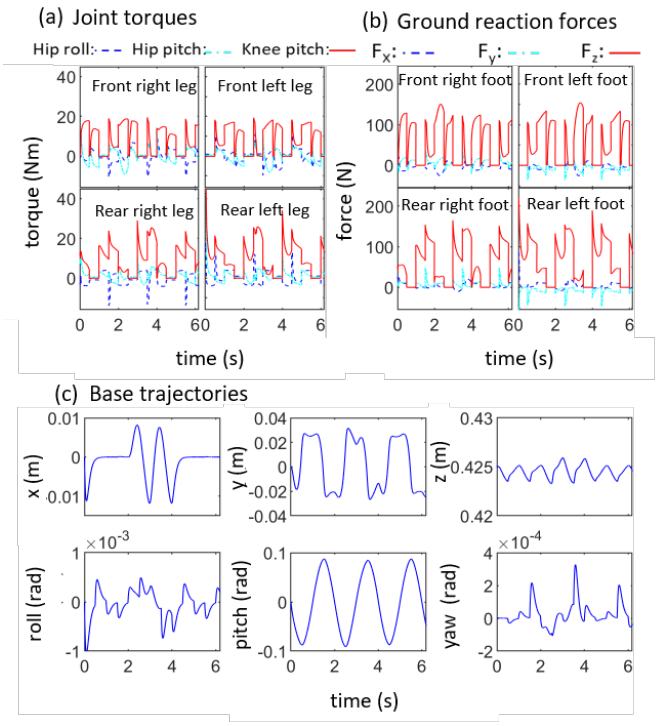

Fig. 6. Simulation results obtained from Case 2 with forward perturbations: (a) joint torques, (b) ground reaction forces, and (c) base trajectories.

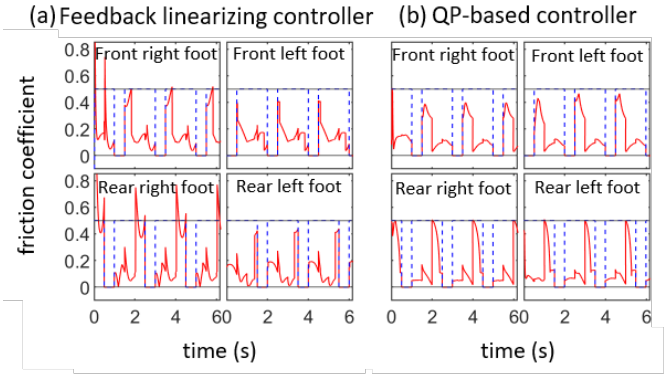

Fig. 7. Comparative simulation results on the satisfaction of the friction cone constraint: (a) our previous offline planning and I-O linearizing control for DRS walking (Iqbal et al., 2020) and (b) the proposed online planning and QP-based control. The friction coefficient of the robot-surface contact is set to be 0.5 in both simulations.

For the lateral perturbation case (see Fig. 5), the robot's base trajectories are notably perturbed between 2 sec and 4 sec, as shown in subplot (c). In particular, the lateral base position trajectory is significantly displaced with a peak deviation of 0.12 m. Similar trends are observed in Fig. 6 (c) for the forward perturbation case. Yet, the proposed planning and controller method is able to sustain stable walking during the perturbations, as well as to drive the actual based trajectories to converge back to the desired motion after the perturbation is over. Also, the joint torque and ground contact constraints are respected throughout the walking process, as demonstrated in subplots (a) and (b) in Figs. 5 and 6.

Case 3 (comparative results). Figure 7 shows the simulation results of our previous offline planning and I-O linearizing control (Iqbal et al., 2020) under unperturbed walking. Although this controller explicitly addresses the surface motion, it relies on offline planning and does not explicitly guarantee the feasibility of ground contact forces. The unilateral ground contact constraint is indeed respected by the controller during simulated walking. Yet, as shown in Fig. 7 (a), the friction cone constraint is violated at the front right and rear right feet. In contrast, the proposed online planning and QP-based control approach is able to respect all ground contact constraints during the unperturbed walking (subplot (a) of Fig. 7), as well as during perturbations (subplots (b) in Figs. 5 and 6).

6. CONCLUSION

In this paper, we have introduced an online planner and QP-based controller design that sustains stable quadrupedal walking on a DRS (e.g., elevators and ships) by explicitly considering the surface motion and guarantees the feasibility of ground contact constraints. The key element of the online planner is a real-time footstep generator synthesized based on the extension of the concept of capture point from stationary surfaces to a DRS. The capture point was derived based on a 3-D LIPM model walking on a DRS that undergoes a constant horizontal velocity and a varying vertical motion. The controller was formulated as a QP based on full-order robot modeling that captures the support foot movement caused by the surface motion as time-varying holonomic constraints. The QP also incorporates other common, necessary constraints (e.g., ground contact constraints) to ensure the feasibility of the real-time controller implementation. The effectiveness of the proposed approach in walking stabilization and disturbance rejection was demonstrated via MATLAB simulations of 3-D quadrupedal walking over a DRS. In our future work, we will validate this approach on a physical quadrupedal robot walking on a real-world nonstationary surface, and extend the approach to ensure locomotion stability and robustness in the presence of uncertain surface movement.

REFERENCES

Asano, F. (2021). Modeling and control of stable limit cycle walking on floating island. In *Proc. of IEEE International Conference on Mechatronics (ICM)*, 1–6.

Barasuol, V., Buchli, J., Semini, C., Frigerio, M., De Pieri, E.R., and Caldwell, D.G. (2013). A reactive controller framework for quadrupedal locomotion on challenging terrain. In *Proc. of IEEE International Conference on Robotics and Automation*, 2554–2561.

Bledt, G., Powell, M.J., Katz, B., Di Carlo, J., Wensing, P.M., and Kim, S. (2018). MIT Cheetah 3: design and control of a robust, dynamic quadruped robot. In *Proc. of IEEE/RSJ International Conference on Intelligent Robots and Systems (IROS)*, 2245–2252.

Caron, S., Escande, A., Lanari, L., and Mallein, B. (2019). Capturability-based pattern generation for walking with variable height. *IEEE Transactions on Robotics*, 36(2), 517–536.

Carpentier, J., Budhiraja, R., and Mansard, N. (2017). Learning feasibility constraints for multi-contact locomotion of legged robots. In *Proc. of Robotics: Science and Systems*, 9p.

Chevallereau, C., Grizzle, J.W., and Shih, C.L. (2009). Asymptotically stable walking of a five-link underactuated 3-D bipedal robot. *IEEE Transactions on Robotics*, 25(1), 37–50.

Englsberger, J., Ott, C., Roa, M.A., Albu-Schäffer, A., and Hirzinger, G. (2011). Bipedal walking control based on capture point dynamics. In *Proc. of IEEE/RSJ International Conference on Intelligent Robots and Systems*, 4420–4427.

Focchi, M., Del Prete, A., Havoutis, I., Featherstone, R., Caldwell, D.G., and Semini, C. (2017). High-slope terrain locomotion for torque-controlled quadruped robots. *Autonomous Robots*, 41(1), 259–272.

Galeani, S., Menini, L., and Potini, A. (2011). Robust trajectory tracking for a class of hybrid systems: An internal model principle approach. *IEEE Transaction on Automatic Control*, 57(2), 344–359.

Gao, Y. and Gu, Y. (2019). Global-position tracking control of a fully actuated nao bipedal walking robot. In *Proc. of American Control Conference*, 4596–4601.

Gao, Y. and Gu, Y. (2019). Global-position tracking control of multi-domain planar bipedal robotic walking. In *Proc. of ASME Dynamic Systems and Control Conference*.

Gu, Y., Yao, B., and Lee, C.S.G. (2018). Exponential stabilization of fully actuated planar bipedal robotic walking with global position tracking capabilities. *Journal of Dynamic Systems, Measurement, and Control*, 140(5).

Hamed, K.A., Kim, J., and Pandala, A. (2020). Quadrupedal locomotion via event-based predictive control and QP-based virtual constraints. *IEEE Robotics and Automation Letters*, 5(3), 4463–4470.

Hutter, M., Gehring, C., Jud, D., Lauber, A., Bellicoso, C.D., Tsounis, V., Hwangbo, J., Bodie, K., Fankhauser, P., Bloesch, M., et al. (2016). ANYmal-a highly mobile and dynamic quadrupedal robot. In *Proc. of IEEE/RSJ International Conference on Intelligent Robots and Systems (IROS)*, 38–44.

Iqbal, A., Gao, Y., and Gu, Y. (2020). Provably stabilizing controllers for quadrupedal robot locomotion on dynamic rigid platforms. *IEEE/ASME Transaction on Mechatronics*, 25(4), 2035–2044.

Iqbal, A., Mao, Z., and Gu, Y. (2021). Modeling, analysis, and control of slip running on dynamic platforms. *ASME Letters in Dynamic Systems and Control*, 1(2).

Joe, H.M. and Oh, J.H. (2018). Balance recovery through model predictive control based on capture point dynamics for biped walking robot. *Robotics and Autonomous Systems*, 105, 1–10.

Kajita, S., Kanehiro, F., Kaneko, K., Fujiwara, K., Harada, K., Yokoi, K., and Hirukawa, H. (2003). Biped walking pattern generation by using preview control of zero-moment point. In *Proc. of IEEE International Conference on Robotics and Automation*, volume 2, 1620–1626.

Koolen, T., De Boer, T., Rebula, J., Goswami, A., and Pratt, J. (2012). Capturability-based analysis and control of legged locomotion, Part 1: theory and application to three simple gait models. *The International Journal of Robotics Research*, 31(9), 1094–1113.

Kuindersma, S., Deits, R., Fallon, M., Valenzuela, A., Dai, H., Permenter, F., Koolen, T., Marion, P., and Tedrake, R. (2016). Optimization-based locomotion planning, estimation, and control design for the Atlas humanoid robot. *Autonomous robots*, 40(3), 429–455.

Lee, J., Hwangbo, J., Wellhausen, L., Koltun, V., and Hutter, M. (2020). Learning quadrupedal locomotion over challenging terrain. *Science robotics*, 5(47).

Li, C., Zhang, T., and Goldman, D.I. (2013). A terradynamics of legged locomotion on granular media. *Science*, 339(6126), 1408–1412.

Morisawa, M., Kajita, S., Kanehiro, F., Kaneko, K., Miura, K., and Yokoi, K. (2012). Balance control based on capture point error compensation for biped walking on uneven terrain. In *Proc. of IEEE-RAS International Conference on Humanoid Robots (Humanoids 2012)*, 734–740.

Pratt, J., Carff, J., Drakunov, S., and Goswami, A. (2006). Capture point: A step toward humanoid push recovery. In *Proc. of IEEE-RAS International Conference on Humanoid Robots*, 200–207.

Pratt, J., Koolen, T., De Boer, T., Rebula, J., Cotton, S., Carff, J., Johnson, M., and Neuhaus, P. (2012). Capturability-based analysis and control of legged locomotion, part 2: Application to M2V2, a lower-body humanoid. *The international journal of robotics research*, 31(10), 1117–1133.

Unitree, R. (2019). Laikago. http://www.unitree.cc/product/. Accessed: 2019-11-28.

Westervelt, E.R., Grizzle, J.W., Chevallereau, C., Choi, J.H., and Morris, B. (2007). *Feedback control of dynamic bipedal robot locomotion*, volume 28. CRC press.

Xiong, X., Ames, A.D., and Goldman, D.I. (2017). A stability region criterion for flat-footed bipedal walking on deformable granular terrain. In *Proc. of IEEE/RSJ International Conference on Intelligent Robots and Systems*, 4552–4559.

Yang, C., Zhang, B., Zeng, J., Agrawal, A., and Sreenath, K. (2020). Dynamic legged manipulation of a ball through multi-contact optimization. In *Proc. IEEE/RSJ International Conference on Intelligent Robots and Systems (IROS)*, 7513–7520. doi:10.1109/IROS45743.2020.9341218.

Zheng, Y. and Yamane, K. (2011). Ball walker: A case study of humanoid robot locomotion in non-stationary environments. In *Proc. of IEEE International Conference on Robotics and Automation*, 2021–2028.